ONSET OF NUCLEATE BOILING, HEAT TRANSFER, VOID FRACTION AND PRESSURE DROP IN SUBCOOLED CONVECTIVE BOILING WITH R12

H. Bräuer, F. Mayinger and G. Stängl

Lehrstuhl A für Thermodynamik, Technische Universität München
Arcisstraße 21, 8000 München 2, FRG

ABSTRACT

Detailed knowledge of th physical phenomena involved in subcooled boiling is of great importance for the design of liquid-cooled heat generating systems with high heat fluxes. Experimental data of heat transfer, void fraction and pressure drop were obtained for forced convective boiling of dichloro- difluoroethane (R 12). The flow is circulated upwards through a concentric annular vertical channel. The reduced pressure studied were $0,24 \leq p/p_{crit} 0,8$, inlet subcooling varing from 10 to 75 K and mass fluxes from 500 to 3000 kg/m^2s, which corresponds to Re numbers from 30 000 to 300 000. For correlating the void fraction in subcooled flow , the drift flux model by *Zuber* was extended, by introducing a new equation for the distribution factor C_o with the Jakob- and Froude-number as variables.

1 INTRODUCTION

The liquid supplied to flow boiling channels is usually in a subcooled state. In such systems, the first occuring heat transfer process is that of convective heat transfer to single-phase flow in liquid form up to the point onset of nucleate boiling (ONB).

These characteristics of subcooled boiling flow have been extensively investigated, but most of the available studies were performed with water. For the conditions of incipient boiling with water, *Sato and Matsumura [1]*, *Bergles and Rohsenow [2]*, and *Davis and Anderson [3]* proposed analytical models based on the existence of cavities on the heated surface. Other investigations dealt with the criteria for the point of net vapour generation and bubble behaviour *[4-8]*, but only limited tests have been carried out on other fluids, especially refrigerants. Using R113, *Hino and Ueda [9]* and, using R11, *Abdelmessih [10]*, observed wall superheating which is independent of the mass flux and inlet subcooling. A more detailed literature review can be found in *[11]*.

2 EXPERIMENTAL SET-UP AND TEST PROCEDURE

The experimental facility, employed in this study, is a closed loop. It is designed to operate with R12, up to the critical pressure. The test section itself, as shown in Fig.1, is a vertically arranged concentric annulus with the inner tube consisting of three sections of the same diameter, one above the other, namely the entrance region, stainless steel heater, and unheated outlet region.

The inner tube has an outer diameter of 16 mm and its heated part is 650 mm long. Heat is supplied at a uniform rate by passing direct electric current through the tube wall. The outer tube is made of a duran glass with inner diameter of 30 mm. The resulting hydraulic diameterof the annulus is 14 mm.

The wall temperatures are measured by 5 shielded Cr-Al thermocouples (diameter of shielding 0,5 mm). These thermocouples are arranged over the length and circumference of the inner tube as also shown in Fig.1. The inlet fluid temperature is measured by two thermocouples, the radial profile of the outlet temperature by three thermocouples. The wall temperature of the outer tube is gaged with ten thermocouples, which are fixed to the wall at different ele-

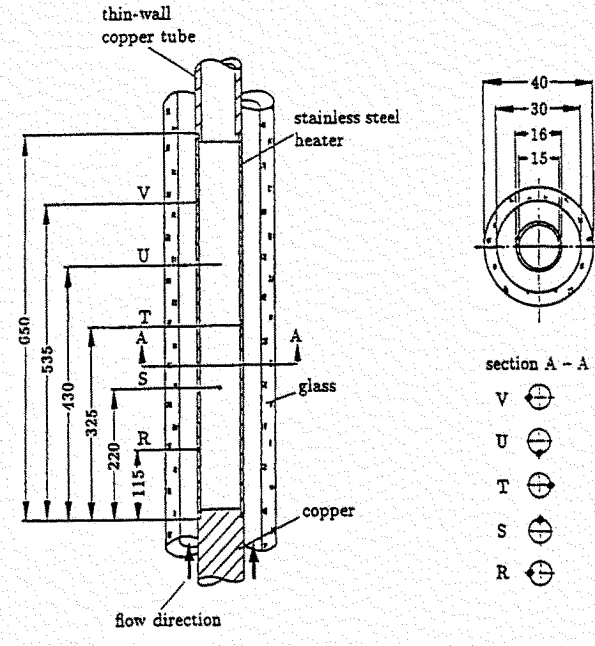

Fig.1 Test section

vations. The whole test section is insulated to yield nearly adiabatic conditions.

The onset of subcooled boiling is measured during slow heating transient, by recording the signals of the thermocouples in the heated wall. At constant systempressure, mass flow rate and inlet subcooling, the heat flux of inner tube in the test section increases slowly and linearly with time. The transient is slow enough to guarantee pseudo-steady conditions over the cross-section by heat conduction in the tube wall and turbulent heat transfer in the fluid. In pure single-phase flow, the heat transfer coefficient is a function of flow conditions only, i.e. it is constant during this period of the heating transient. Therefore, the wall temperatures increase linearly with time. When subcooled boiling starts, the heat transfer coefficient suddenly undergoes a step change, which is observed as a break in the plot of temperature versus time. With R12, this break is so pronounced that even a stepwise temperature decrease can be seen at the exact moment at which subcooled boiling starts, as demonstrated in Fig.2, where the wall temperature and heat flux are plotted versus time. With continuing heat supply, the boiling zone expands upstream, downwards and when the signal of the thermocouple "R", see Fig.1, indicates that the nucleate boiling has reached the entrance region, the maximum heat flux for this particular run has been achieved. In order to check the wall temperature behaviour when boiling is terminated and the heat transfer mode changes from boiling to single-phase convection, the heat flux is temporarily reduced in the same way as described above until boiling is terminated. Obviously, no temperature jump does occur now when subcooled boiling subsides but the wall temperature decreases continuously with decreasing heat flux.

A single beam γ-densitometer is used to measure the radial void distribution and, subsequently, to evaluate the integral void fraction in a cross section, as well as to compare γ-source data with imped ance void fraction data. The γ-source comprises a Cs 137 radiator in a lead shielding. The outlet of the source and the inlet of the detector are sharply collimated to a height of 30 mm and a width of 1 mm. This is to guarantee that the beam passes through a well-defined control volume. The γ-densitometer set-up is mounted on a table which can be moved vertically and

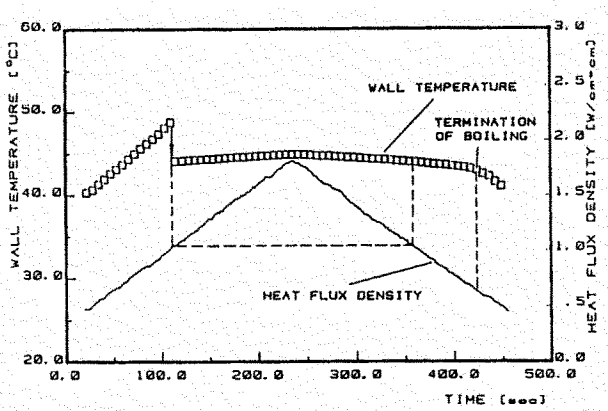

Fig.2 Wall temperature and heat flux density profile

radially. Accordingly, measurements can be taken at any point of the test channel.

To measure relatively low void fractions, which occur during subcooled boiling, a special impedance probe set-up has been designed. Eight of these impedance probes are installed at different elevations in the test section. Fig.3 illustrates the probe design. The outer electrode of the measuring capacitor is represented by a brass ring of 20 mm length mounted flush with the outer tube of the annulus section. The heated inner tube of the annulus serves as counter electrode of the capacitor. Above and below each so-called guard rings are arranged, supplied by the same electric circuit as the measuring electrode, which make the electric field in the measuring capacitor as homogeneous as possible. Both measuring ring and guard rings are held in a resin, which is resistant to Freon 12 even up to relatively high temperatures. The vessel of the probe is made of stainless steel with two cable connections for the signal cable and the guard signal cable, respectively. The probe and the ring with a pressure tap are fixed between two flanges. One of the impedance probes is mounted in the unheated inlet section of the test tube. Shortly above the lower end of the heated section, a set of four impedance probes is mounted within a short distance of each other, to obtain void fraction data at the onset of nucleate boiling. The three other probes are distributed in equal distance along the remaining length of the heated section.

Fig.4 illustrates the electric circuit supplying the impedance void probes. The guard rings are supplied with an electric field of the same phase, amplitude and frequency as the measuring electrode, thus avoiding stray capacity of the measuring capacitors' field. The impedance probe, which is mounted in the unheated section of the test tube, serves as

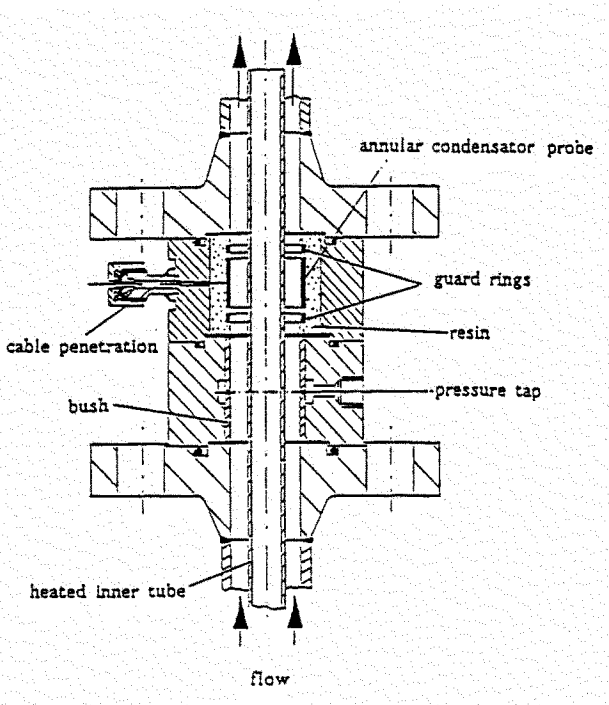

Fig.3 Design of the impedance void probe

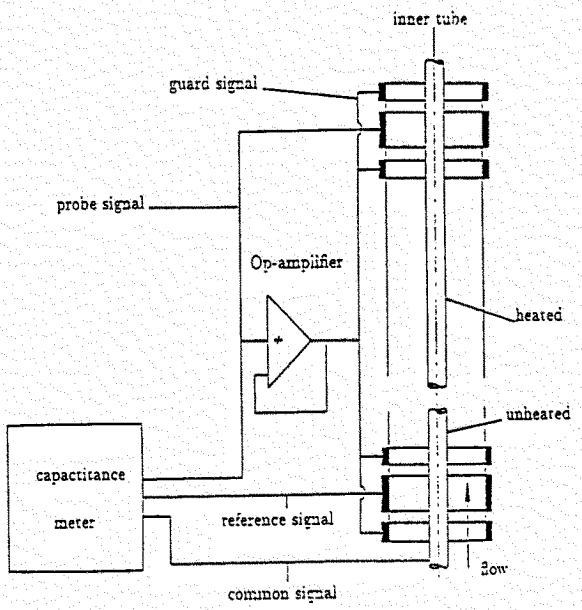

Fig.4 Electrical circuit of the void meter

a reference probe in the way that the measured capacitance value represents the difference between the capacitances of the reference probe and the considered measuring probe in the heated area. The accuracy of the measured value can be largely increased by using this differential method.

The pressure drop profile along the test section is measured by four strain gage differential pressure transducers. Separation vessels are mounted outside the test section in the same level as the pressure traps to avoid bubbles in the measuring tubes, which can cause a measuring error. At the top and bottom of the measuring tube, thermocouples are installed to gage the temperature in these tubes, which is needed for the later correction of the measured values becoming necessary due to the hydrostatic pressure in the tubes.

The radial temperature profile was measured with a moveable temperature probe fixed in the test section at an elevation of 1.045 m above the beginning of the heated section of the test tube. The probe is electrically insulated from the outer tube to prevent an electric shock, which could damage the built-in themocouple. The actual temperature is measured with a coated cromel-alumel themocouple with a diameter of 0.25 mm. This thermocouple can be moved inside the gap between the outer and the heated inner wall in steps of at least 0.1 mm pitch.

3 ANALYSIS OF ONSET OF SUBCOOLED BOILING

3.1 The Boiling Hysteresis Phenomenon

During heating, as soon as incipient boiling is initiated, a sharp drop in wall superheating takes place. After this jump, the measured curve is close to that of fully developed boiling. The temperature profile for decreasing heat flux follows that generated by increasing the heat flux until boiling. The temperature profile for decreasing heat flux follows that generated by incresing the heat flux until boiling is terminated. From this point, the curve continues to decline smoothly, to merge with the single-phase forced convection curve. This behavoiur is traditionally referred to as "hysteresis" and is even more clearly demonstrated in Fig.5, where the heat flux is plotted against the wall superheating for two different mass flow rates.

For boiling water, this considerable wall superheating has not been reported in literature. To explain this difference, a comparison of some physical properties of water with those of R12 is shown in Table 1. The basis of comparison was the reduced pressure.

Table 1 shows that the surface tension of water is more than triple that of R12. Therefore, it can be assumed that, in R12, the larger cavities on the heated wall will probably be flooded, i.e. wetted and filled with liquid prior to incipient boiling and are, therefore, not available for nucleation. If this is the case, the residual volume in those cavities, which are not flooded, is very small and a correspondingly high superheatingis required to activate these cavities. This may be an explanation of the measured high wall superheating needed for the activation of boiling in R12, as shown in Fig.5.

Table 1. Physical properties of water and refrigerant R12 at reduced pressure presure p/p_{crit} in the range $0 \leq p/p_{crit} \leq 0.75$, according to [12]

μ_{H_2O}	=	$0.466\ \mu_{R_{12}}$	[kg/m s]
k_{H_2O}	=	$7.330\ k_{R12}$	[W/m K]
σ_{H_2O}	=	$3.242\ \sigma_{R_{12}}$	[N/m]
Δh_{vH_2O}	=	$12.14\ \Delta h_{vR_{12}}$	[J/kg]
Pr_{H_2O}	=	$0.33\ Pr_{R_{12}}$	[-]

3.2 Regression Analysis

In order to formulate a correlation for calculating the onset of necleate boiling as a function of thermal and hydrodynamic parameters used in the present experiments, an empirical exponential equation of the following type was chosen:

$$Bo = CRe^{a}\left(\frac{p}{p_{crit}}\right)^{b} Ja_{mod}^{c} \qquad (1)$$

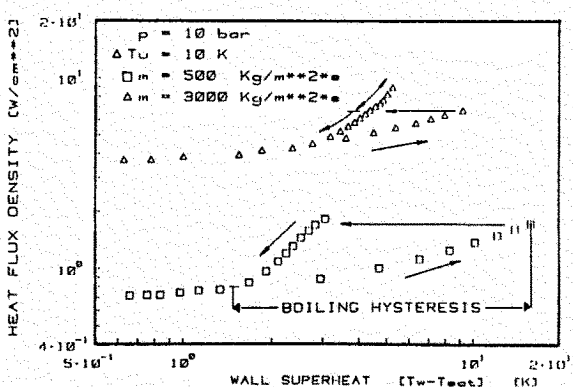

Fig.5 Boiling curves at different mass flux densities

The Bo number

$$Bo = \frac{q_{onb}}{m\Delta h_v} \tag{2}$$

in Eq. (1) includes two parameters of main influence, namely The heat flux and the mass flux, whereas the Re-number

$$Re = \frac{mD_h}{\mu} \tag{3}$$

reflects the influence of the velocity profile.

Furthermore, the reduced pressure (p/p_{crit}) is used as a scaling parameter for modelling the thermodynamic parameters of different fluids.

The variable degree of subcooling is taken into account in the modified Ja-number

$$Ja_{mod} = \frac{h_s - h_b}{\Delta h_v}\frac{\rho_l - \rho_g}{\rho_g} \tag{4}$$

To determine constant C and exponents in Eq. (1), a stepwise multiple regression analysis was employed. The result of this calculation is summarized in Eq. (5).

$$Bo = 0.0015 Re^{0.112}\frac{p}{p_{crit}} Ja_{mod}^{0.773} \tag{5}$$

In the first consideration, it is astonishing that the exponent on the Re number in (5) is negative and, as a result, the mass flow rate also has a negative exponent. Taking into account the fact that the mass flux is included in the denominator of the Bo number as well, the resultant exponent on the mass flux will be 0,89 and this value is in good agreement with the correlations from literature for single-phase flow.

Fig.6 shows how equation (5), based on our own experimental data, agrees with measured data in the literature *[10 - 18]*, taking in account also experiments in water.

4. VOID FRACTION AND PRESSURE DROP

4.1 Void fraction

In Fig.7 the volumetric void fraction, gaged with the impedance void meter, is plotted versus the equilibrium quality defined by

$$x_{eq} = \frac{h_L - h_{SL}}{h_{LG}} \simeq \frac{c_p(T(z) - T_s)}{h_{LG}} \tag{6}$$

where T(z) is the mean bulk temperature (according to *Dix [19]*) at the axial position z. Fifteen data sets are plotted together in this figure. They were measured at the same reduced pressure $p/p_c = 0.48$ and the same mass flux $\dot{m} = 500\ kg/m^2s$. For a set of five of these test runs the inlet subcooling has been varied from 10 to 50 K. The data sets illustrated in Fig.7 allow to see the void formation over a wide range of calculated equilibrium qualities. Analysing the results one can see that, after a small increase at the beginning of vapor formation, the void fraction is nearly constant over a wide range of the equilibrium quality until a point of significant vapor generation (please refer to *[7]*) is reached. This behaviour can be explained by the fluiddy-

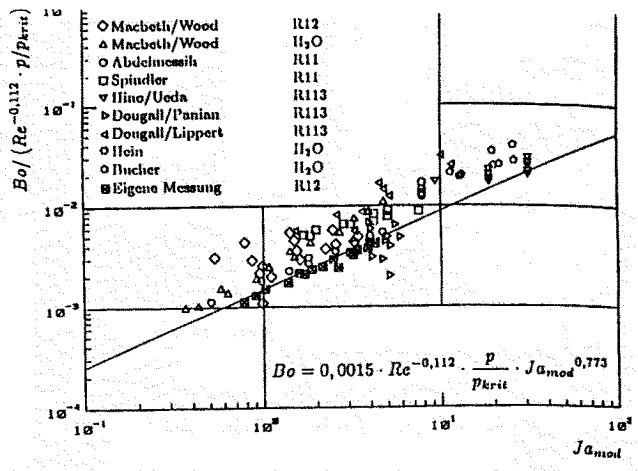

Fig.6 Comparisson of our correlation with data from other authors

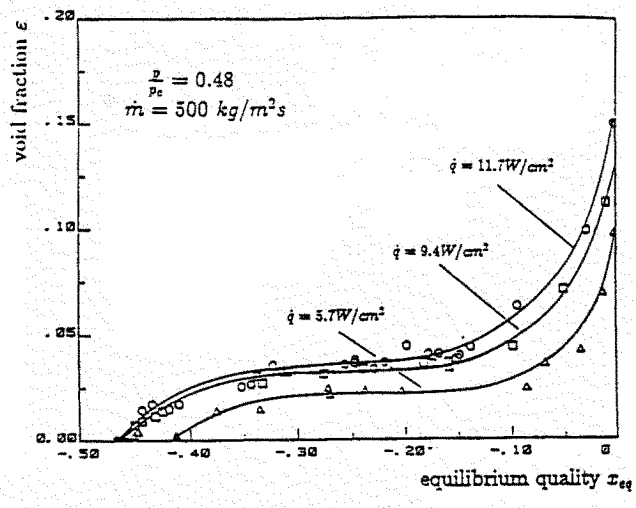

Fig.7 Void fraction formation at various heat flux densities

namic behaviour of the bubbles. At very high subcoolings, the bubbles remain attached to the wall and recondense at the place they grew, due to the very thin superheated or saturated liquid layer. Consequently, the void fraction is high at a given equilibrium quality x_{eq}, because the slip S (eq.7) is zero. The slip is defined by

$$S = \frac{u_G}{u_L} \tag{7}$$

With decreasing subcooling some bubbles grow larger and are able to detach from the heated surface, due to the drag and bouyancy forces, which exceed the attaching force of the surface tension. So the detaching bubbles slide along the bubble layer and flow with the bulk, where they condense. Eventually, the slip approaches 1 and finally exceeds 1, which means that the bubbles start to travel faster than the liquid, resulting in a phase separation. A reason for the almost constant void fraction in this zone, inspite of increased evaporation, is increasing condensation due to the better heat transfer between the moving bubbles and

the subcooled liquid. In a range from -0.1 to 0 of the equilibrium quality, the vapor production exceeds the recondensation rate. A variation of the mass flux density is given in Fig.8. In this figure three diverent mass flux densities are plotted together gaged at the same pressure and heat flux density. The void fraction decreases with increasing mass flux. The arrow placed at the x_{eq} axis indicates the calculated onset of nucleate boiling using equation (5) for the mass flux of $\dot{m} = 2500\ [kg/m^2s]$.

An example of the radial void profil measured with the γ ray attenuation and of the radial temperature distribution in the fluid is given in Fig.9, where the mass flux density was set to $\dot{m} = 1500\ kg/m^2s$, the reduced pressure to $p/p_c = 0.48$ and the heat flux density to $\dot{q} = 7.5\ W/cm^2$. The void fraction data are indicated by circles, the temperature data by crosses. These three plots illustrate the vapor formation at different inlet subcoolings.

The true vapor quality $\dot{x}$ defined by

$$\dot{x} = \frac{\dot{M}_G}{\dot{M}} \tag{8}$$

with the total mass flow ($\dot{M}$) and the vapor mass flow ($\dot{M}_G$), can be calculated by using an energy balance and the balance of momentum. In our calculations the energy balance was based on the measurements of the temperature profile (Fig.9) which however had to be corrected. This correction had been done using the method proposed by lit Staub [24] To fit the data, the well known drift flux model, proposed by *Zuber and Findlay [22]*, was used. In this model, the relationship of the volumetric void fraction ε and the true quality $\dot{x}$ is given by

$$\varepsilon = \frac{\dot{x}/\varrho_G}{C_0[\dot{x}/\varrho_G + (1-\dot{x})/\varrho_L] + V_{jg}/\dot{m}} \tag{9}$$

where V_{jg} is the vapor drift velocity and C_0 the distribution

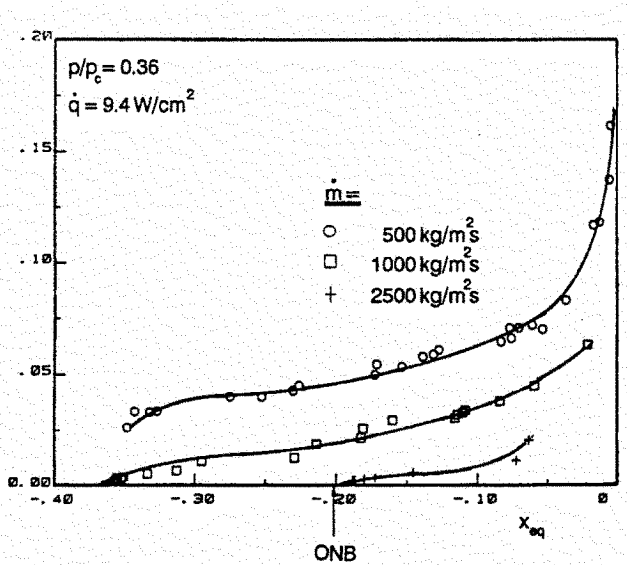

Fig.8 Void fraction formation at various mass flux densities

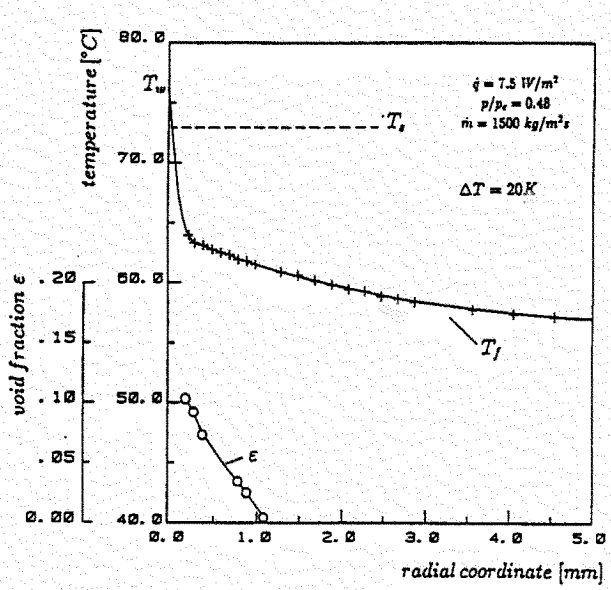

Fig.9 Radial temperature profile and local void fraction at $\Delta T = 20K$

parameter. The drift velocity V_{jg} was set to

$$V_{ig} = 1.18\left[\frac{\sigma g(\rho_L - \rho_G)}{\rho_L^2}\right]^{0.25} \tag{10}$$

with the surface tension (σ) and the acceleration due to gravity (g). Using a stepwise regression analysis of the data, measured in the above discribed test section and the stutation data published by *Friedel [23]*, the distribution parameter C_0 was fit to

$$Co = \dot{\varepsilon}\Big[1 + 1.049Fr^{-0.05}(1-Ja)^{0.164} \left(\frac{\rho_G}{\rho_L}\right)^{0.694} \left(\frac{1-\dot{x}}{\dot{x}}\right)\left(1-\frac{p}{p_c}\right)^{0.124}\Big] \tag{11}$$

with the average volumetric flow concentration $\dot{\varepsilon}$ defined by

$$\dot{\varepsilon} = \frac{1}{1 + \frac{1-x}{x}\frac{\rho_G}{\rho_L}} \tag{12}$$

In consideration of the geometry and the mass flux, the Froud number

$$Fr = \frac{\dot{m}^2}{g d_{hy} \varrho_L^2} \tag{13}$$

was included. To indicate the degree of subcooling, i.e. the inlet subcooling of the fluid, the Jacob number was inserted, which is defined by

$$Ja = \frac{h_{SL} - h_{in}}{h_{LG}} \tag{14}$$

Fig.10 illustrates the measured quality $\dot{x}$, gaged and calculated at a mass flow rate $\dot{m} = 500\ kg/m^2s$ at several heat flux densities and pressures, which is plotted versus the volumetric void fraction. The lines indicate the calculated void fraction with eq.9 using the distribution parameter C_0 calculated with eq.11.

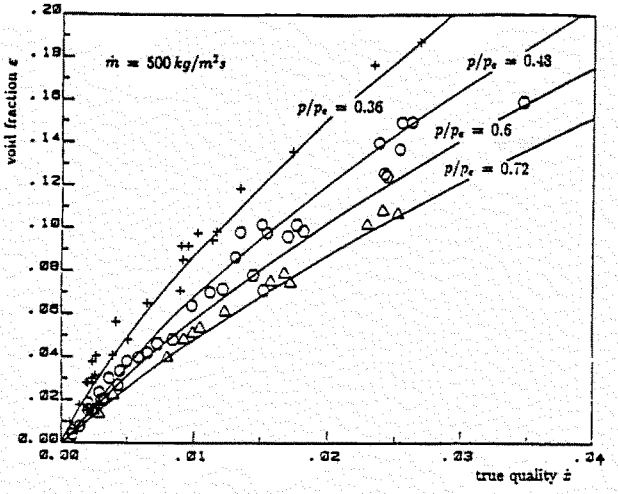

Fig.10 True quality and void fraction at different pressures

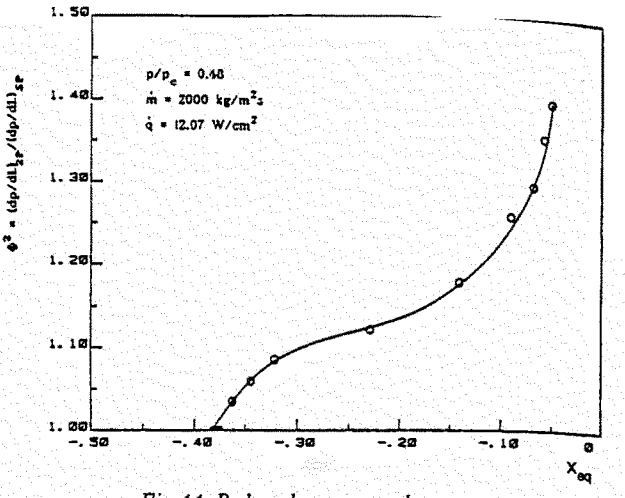

Fig.11 Reduced pressure drop

4.2 Pressure Drop

In order to receive information about the single phase friction factor, some single liquid flow experiments under adiabatic conditions have been conducted. The obtained friction factor for the considered geometry shows a good agreement with the equation proposed by *Deubel [24]* for single phase liquid flow in an annulus. Therefore, the correlation can be generally used to quantify the ratio of the two phase pressure gradient (given in eq.15).

$$\Phi^2 = \frac{(dp/dz)_{2p}}{(dp/dz)_{sp}} \qquad (15)$$

The pressure drop in subcooled boiling qualitatively shows a similar behaviour to the void fraction versus the subcooling, respectively versus the flow path. In Fig.11 the Martinelli two-phase flow multiplier (defined in eq.(15) is plotted versus the subcooling, represented by the equilibrium quality x_{eq}. The data were taken at a mass flux density of $\dot{m} = 2000\ kg/m^2s$, a reduced pressure of $p/p_c = 0.48$ and a heat flux of $\dot{q} = 12.07\ W/cm^2$. The bubble "coating" at the wall displaces the liquid and reduces its flow area. The resulting higher velocity and especially the momentum exchange with the bubble "coating" leads to a pronounced increase in the pressure drop at the onset of subcooled boiling. Here we have to realize that each activated bubble grows and recondenses within a few microseconds and always presents a small, but violent obstacle in the flow. Upstream or at lower subcooling bubbles can separate from the wall and travel with the liquid, so their influence as an obstacle is reduced. Therefore, the pressure drop curve in this area is less steep. Another reason for this flattening of the pressure drop curve is the fact that the bubbles still condense in the subcooled liquid and their decrease in volume and final disappearance has an accelerating effect to the liquid. Finally, with strongly increasing void fraction - at low subcooling - the pressure drop increases exponentially and, as we saw in Fig.7, analogous to the void fraction.

REFERENCES

[1] **Sato, T. & Matsumura, H.**, *Bull. Jpn. Soc. Mech. Eng.* 7 (1964) pp. 392 - 398.

[2] **Bergles, A.E. & Rohsenow, W.M.**, *Trans. ASME*, Ser. C 86 (1964) pp. 365 - 372.

[3] **Davis, E.J. & Anderson, G.H.**, *AIChE J.* 12 (1966) pp. 774 -780.

[4] **Levy, S.**, *Int. J. Heat mass Transfer* 10 (1967) pp. 951 -965.

[5] **Staub, F.W.**, *Trans. ASME*,Ser. C 90 (1968) pp. 151 - 157.

[6] **Sara, O. & Zuber, N.**, *Proc. 5th Int. Heat Transfer Conf., Tokyo 4*, (1974), pp. 175 -179.

[7] **Bjorge, R.W. , Hall, G.R. & Rohsenow, W.M.**, *Int. J. Heat Mass Transfer*,25 (1982) No.6,pp. 753 -757.

[8] **Seoguchi, K., Nishikawa, K., Nakasatomi, M., Hirata, N. & Higuchi, H.**, *Proc. 5th Int. Haet Transfer Conf., Tokyo 4*, (1974), pp. 180 - 184.

[9] **Hino, R. & Ueda, T.**, *Int. J. Multiphase Flow* 11, (1985) No. 3, pp. 296 -281.

[10] **Abdelmessih, A.H. , Fakhri, A. & Yin, S.T.**, *Proc. 5th Int. Heat Transfer Conf., Tokyo 4*, (1974), pp. 165 - 169.

[11] **Butterworth, D. & Shock, R.A.**, *Proc. 7th Int. Heat Transfer Conf., Munich 1*, (1982), pp. 11 - 30.

[12] **Mayinger, F.** „Strömung und Wärmeübergang in Gas-Flüssigkeits-Gemischen", Springer - Verlag, Wien, New York, 1982.

[13] **Spindler, K. & Hahne, E.**, *Chem.-Ing.-Technik*, Bd.60, Nr.1, (1988), pp. 54 - 55.

[14] **Macbeth, R.V. & Wood, R.W.**, *European Two-Phase Flow Group Meeting, Univ. Strathclyde*, 1980.

[15] **Dougall, A.S. & Lippert, T.E.**, *NASA Rep.*, GR - 2241, 1973.

[16] **Dougall, R.S. & Panian, D.J.**, *NASA Contractor Report*, GR - 2137, Washington, D.G., 1972.

[17] **Bucher, B.**, Diss. Universität Hannover, 1979.

[18] **Hein, D. & Köhler, W.**, *Report* Nr. 43.02.05, MAN, 1968.

[19] **Dix, G.E.**, Ph.D. Thesis Univ. of California, 1970

[20] **Jain, P.K., Nourmohammadi, K. & Roy R.**, *Nuc. Eng. and Des.*, 60, 1980.

[21] **Staub, F.W., Walmet, G.E. & Niemi, R.O.**, *Final Report NYO-3679-8*, 1969.

[22] **Zuber, N. & Findlay, J.A.**, *J. of Heat Transfer,*, 87, 1965.

[23] **Friedel, L.**, Diss. Uni. Hannover, 1974.

[24] **Deubel, K.L.**, Diss. TU Darmstadt, 1964.